Nuclear Instruments and Methods in Physics Research A 1067 (2024) 169674

Contents lists available at ScienceDirect

Nuclear Inst. and Methods in Physics Research, A

journal homepage: www.elsevier.com/locate/nima

Full Length Article

Ion-optical simulations for the NEXT solenoid separator

A. Soylu [a], X. Chen [a], J. Even [a,*], A. Karpov [b], V. Saiko [b], J. Sarén [c], J. Uusitalo [c]

[a] Van Swinderen Institute for Particle Physics and Gravity, University of Groningen, Groningen, 9747AA, The Netherlands
[b] Flerov Laboratory of Nuclear Reactions, Joint Institute for Nuclear Reseach, Dubna, 141980, Russia
[c] Department of Physics, University of Jyväskylä, Jyväskylä, 40014, Finland

ARTICLE INFO

MSC:
00-01
99-00

Keywords:
Ion-optical simulations
Solenoid separator
Multinucleon transfer
In-flight separation
NEXT

ABSTRACT

In this paper, we present ion-optical simulation for the design studies of a new solenoid separator as part of the NEXT experiment. Our aim is to separate Neutron-rich, EXotic, heavy nuclei produced in multinucleon Transfer reactions (NEXT) from the primary beam and un-wanted by-products within the magnetic field. The goal of the simulation is to find the optimum arrangement of the components within the NEXT solenoid separator to achieve the highest transmission efficiencies of transfer products and a good suppression of background. In our simulations, we focused on two complementary reactions to produce transfermium isotopes and to produce neutron-rich nuclei around the neutron number $N = 126$. Transmission yields above 50% for the transfermium isotopes of interest were reached in the simulations. The simulated yields for $N = 126$ lie between 5% and 20%.

1. Introduction

Multinucleon transfer (MNT) reactions provide access to some neutron-rich isotopes which are hard to reach through other types of nuclear reactions. Multinucleon transfer takes place in a deep inelastic collision of a projectile and a target nucleus at energies around the Coulomb barrier. The transfer products are emitted in a large solid angle mainly in forward direction. The angular distribution of the MNT products peaks near the grazing angle [1]. However, due to the wide angular distribution experimental studies are challenging and require setups with large angular acceptances. Even the large solid angle spectrometers like PRISMA [2], and VAMOS++ [3] are only able to cover a small section of the solid angle. Setups like KISS [4], the $N = 126$ factory [5], the IGISOL experiments at Jyväskylä [6], and MNT studies at the FRS gas-catcher [6] cover a large fraction of the reaction products by placing gas cells behind the target. These approaches require additional separation steps or even re-ionization to perform precision studies of the transfer products. An alternative method is a chemical separation [7] of the transfer products, which can only access long-lived isotopes with half-lives in the range of minutes or hours. We are currently building a new experimental setup called NEXT to study Neutron-rich, EXotic, heavy nuclei produced in multinucleon Transfer reactions using a large solenoid magnet to separate and focus transfer products. Within the experimental program of NEXT, we will focus on reactions using light to medium heavy ion beams such as argon, nickel, calcium, or xenon and heavy targets such as platinum, lead, or actinides. Our interest lies on heavy target-like transfer products that are created in this type of reactions. Specifically, we will focus on nuclei around the closed neutron-shell $N = 126$ which are accessible in reactions induced by ^{136}Xe beam as well as neutron-rich transfermium isotopes, which can be produced in reactions of medium heavy projectiles and actinide targets. Our goal is to measure the masses of the heavy transfer products with highest precision to serve as benchmark data for nuclear mass models and nuclear astrophysics. Furthermore, we plan to perform decay spectroscopy of isobarically purified samples, and identify long-lived transfermium isotopes which decay through spontaneous fission.

1.1. The NEXT experiment

The NEXT setup is installed at the PARTREC facility in Groningen. Fig. 1 shows the schematic of the NEXT setup. The primary ion beam will be delivered by the AGOR cyclotron. The target will be placed inside a solenoid magnet. The pressure inside the solenoid separator is below 10^{-5} mbar. The unreacted primary beam and reaction products emitted in a small angle will be stopped by a Faraday cup. The light and heavy transfer products will be separated as indicated in Fig. 1. The projectile-like fragments will hit the walls of the solenoid magnet, while the target-like products will be focused towards the end of the solenoid magnet and stopped in a gas-catcher [8]. The cooled-down products will be extracted from the gas-catcher and will be transported by a RadioFrequency (RF) ring-ion guide and buncher [9]. Subsequently,

* Corresponding author.
E-mail address: j.even@rug.nl (J. Even).

https://doi.org/10.1016/j.nima.2024.169674
Received 16 January 2024; Received in revised form 24 July 2024; Accepted 29 July 2024
Available online 12 August 2024

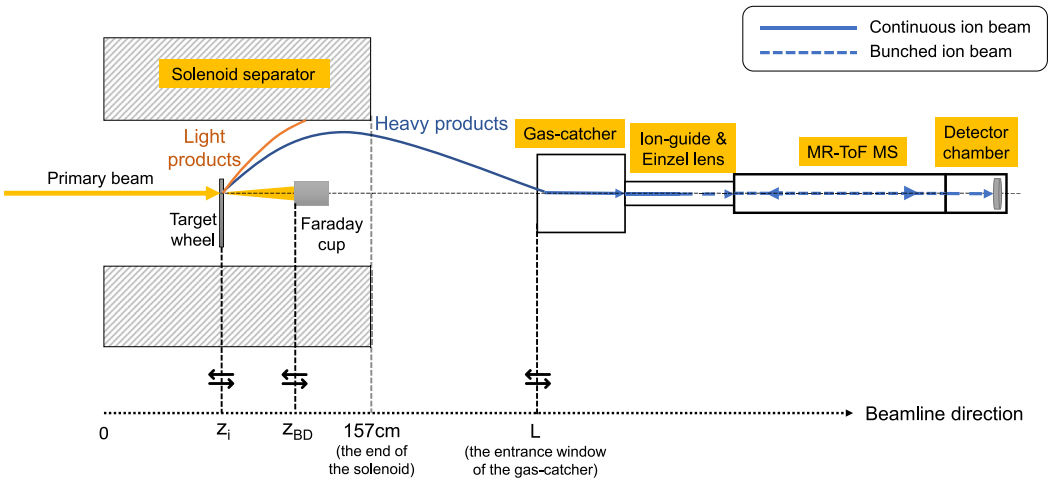

Fig. 1. Schematic of the NEXT experiment. The primary beam delivered by the AGOR cyclotron is focused on the target which is placed inside the solenoid magnet. The unreacted beam and products emitted within a small angle are stopped on a Faraday cup. The light projectile-like products hit the wall, while heavy target-like products are guided towards the end of the solenoid and stopped inside the gas-catcher. From there, the heavy transfer products are extracted and guided towards the MultiReflection Time-of-flight Mass Spectrometer (MR-ToF MS).

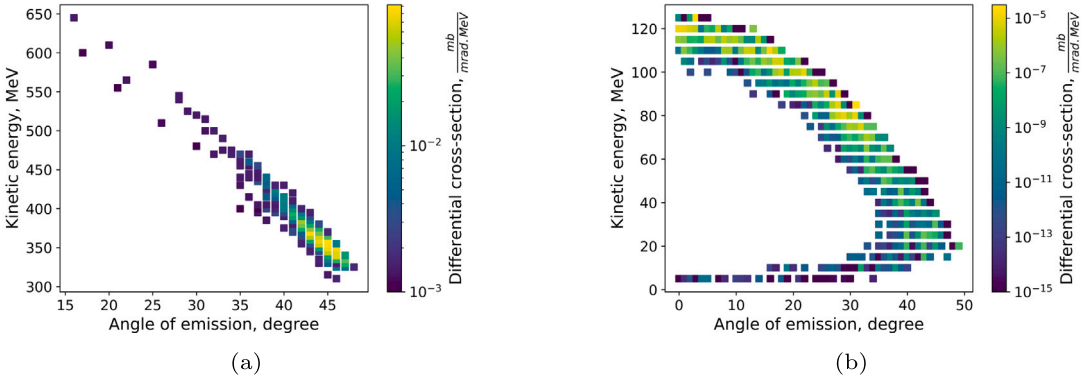

Fig. 2. Theoretical predicted kinematic distribution of (a) ^{203}Ir produced in ^{136}Xe+^{198}Pt, and (b) ^{261}Md produced in ^{48}Ca+^{251}Cf.

the ions will be injected into a Multi-Reflection Time-of-Flight Mass Spectrometer (MR-ToF MS) [10,11] for isobaric separation and mass measurements. A detector for background-free spectroscopy will be placed behind the MR-ToF MS.

1.2. Aim of the ion-optical simulations

In this paper, we present the simulations of the ion trajectories through the solenoid separator. A Python [12] script (see Section 2) has been developed that allows to reconstruct the magnetic field inside the solenoid and the fringe field extending far from the physical boundaries of the solenoid as described in Section 2.1. It provides the flexibility to implement obstacles such as the Faraday cup inside the magnetic field. The input parameters such as the total kinetic energies of the ions, their angles of emission, and differential production cross-sections can be read directly from a data file into the code. The calculation of the atomic charge state distribution has been implemented in the code (see Section 2.2). The trajectories of ions depend on their angle of emission and magnetic rigidity,

$$B\rho = \frac{\upsilon m}{q} \tag{1}$$

where ρ is the gyroradius of the ion, υ is its velocity, m is its mass and q is its atomic charge state. Only ions with an angle of emission and magnetic rigidity that are covered by the acceptance region of the solenoid separator will be transmitted from the target towards the gas-catcher. Ions outside the acceptance region will be suppressed (see Section 3).

To optimize the design of the separator we chose two model reactions:

- ^{136}Xe+^{198}Pt at 6 MeV/u, (see Section 3.1)
- ^{48}Ca+^{251}Cf at 6.1 MeV/u, (see Section 3.2)

The reaction ^{136}Xe+^{198}Pt at 6 MeV/u was studied as an example for a symmetric transfer reaction to produce nuclei around $N = 126$ shell closure [13]. The reaction ^{48}Ca+^{251}Cf at 6.1 MeV/u was selected as a typical case for an asymmetric reaction to produce nuclei in the transfermium region [14]. For both reactions, data predicted by theory [13,14] were used for the simulations. The data sets include the atomic numbers (Z_p), mass numbers (A_p), angle of emission (θ), kinetic energy (KE), and differential cross-section (σ) of the reaction products and scattered target and beam particles. Both reactions feature relatively wide angular distributions of the transfer products. The highest production cross-sections are obtained for the transfer of one or two nucleons between target and projectile. The differential cross section for the production of neutron-rich target-like fragments at $N = 126$ in ^{136}Xe+^{198}Pt peaks at recoil energies of 350 MeV to 400 MeV and at an angle of emission around 40°. The proton-rich and heavier target-like transfer products of this reaction are mainly emitted in smaller angles and at higher kinetic energies.

The neutron-rich transfermium isotopes that are produced in ^{48}Ca+^{251}Cf feature smaller angles of emission of around 10° to 30°,

their kinetic energies peak around 50 MeV to 100 MeV. Fig. 2 shows the theoretical prediction of the angular and energy distribution of ^{203}Ir produced in ^{136}Xe+^{198}Pt, and of ^{261}Md produced in ^{48}Ca+^{251}Cf, energy losses in the target are not taken into account.

Based on the data sets provided by theory we optimized the acceptance region of the NEXT separator by adjusting the positions of the target wheel, the Faraday cup, and the gas-catcher to achieve a high transmission yield of the isotopes of interest and a good separation of unwanted by-products. Additionally, we verified in TRIM simulation [15] that scattered primary beam is stopped on the Faraday cup. In the following sections, we will provide an overview of the structure of the Python code, explain its features, and present the results of our simulations for the chosen reactions.

2. The simulation code

The flowchart of the algorithm of the simulation is illustrated in Fig. 3. In the first step, the user defines the initial conditions of the simulation such as the atomic number of the target material (Z_t), the position of the target(r_i, z_i) from where the ions are released, two step size of the displacement of the ion- the macroscopic step in axial direction (Δz) to check for collisions with the walls and obstacles and to plot the trajectories as well as a microscopic maximum step (Δt) for the integration of the equation of motion in time. Furthermore the user defines the maximum length of the ion trace (L), the inner radius of the solenoid magnet (r_{sol}), the length (L_{sol}) of the solenoid magnet, and the number of ions (n) per charge-state-distribution. It is possible to implement radially symmetric obstacles such as the Faraday cup or the walls of the magnet (r_{sol}) in the code. The geometry of the obstacle is defined by its length (z_{BD_1}, z_{BD_2}) and radius (r_{BD}). In the second step, a magnetic field of a solenoid magnet is calculated as described in Section 2.1. The script imports the theoretically predicted data of the reaction kinematics from a csv (comma-separated values) file. The data file includes a list of values of the atomic number (Z_p), mass number (A), angle of emission (θ), kinetic energy (KE), and differential cross-section (σ) values of the various reaction products. Every isotope defined by A and Z_p is processed separately. The code selects first the element with the lowest atomic number (Z_p) from the list, afterwards it picks the isotope with the lowest mass number (A). The code generates distributions of atomic charge states (see Section 2.2) for every pair of kinetic energy and angle of emission listed in the input data file for the selected isotope. Each distribution of charge states contains x number of ions. A weighting factor based on the differential cross section ($w_n = \sigma_n/n$) is assigned to all ions. All the generated ions are combined into one array (X). The traces of the ions are simulated step by step along the magnetic field. The value of the microscopic step size Δt was chosen so that the error of the integration is less than 0.1 mm. The step size (Δz) is typically around 5 mm and can be adjusted by the user. The equation of motion is numerically integrated by a self-implemented second-order Runge–Kutta method [16] with a fixed step size, which allows to vectorize the calculation of the displacement of all ions in axial (Δz) and radial direction (Δr) within the Numpy [17] numerical library. As soon as an ion hits an obstacle its trajectory is terminated. Terminated ions are moved from the array X to the array X'. The process continues until all ions have either hit the wall or an obstacle or if the position of all ions along the beam axis reaches the maximum length along the z-axis of the ion trace calculation (L) which corresponds to the position of the gas-catcher. All traces of ions that reach L are saved in a file. In the following step, the next heavier isotope ($A+1$) is selected from the input file and the process repeats. After the heaviest isotope (A_{max}) is processed, the code picks the next element with a higher atomic number ($Z+1$) and the simulation process repeats until the element with the highest atomic number (Z_{max}) from the file has been processed. After the simulation is completed, the data of the ion traces such as positions, directions, velocities of the ions can be extracted.

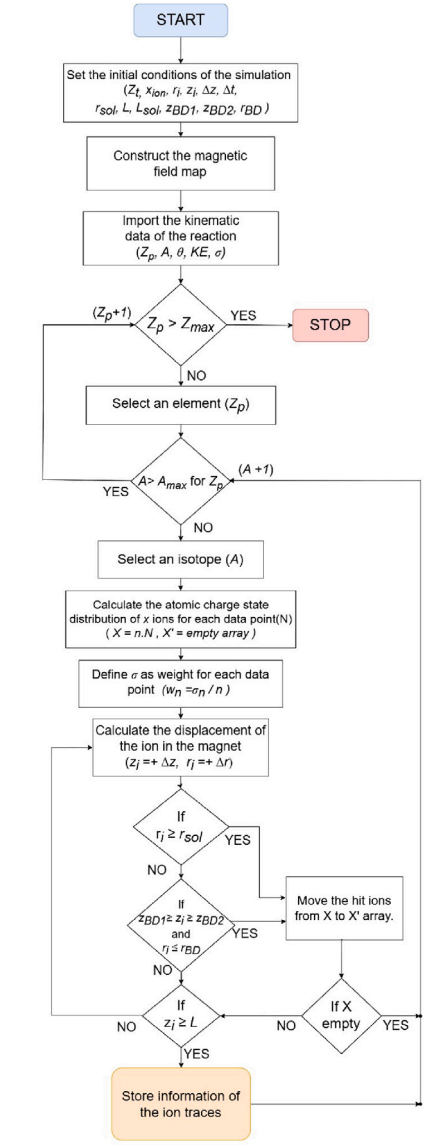

Parameters:
Z_t: Atomic number of the target material
n: Number of ions
r_i, z_i: Position of the target
Δz, Δr: Step size in the axial, radial direction
Δt : Maximum step for the integration of the equation of motion in time.
r_{sol}, L_{sol}: Inner radius and the length of the magnet
L: Maximum length of the ion trace
z_{BD1}, z_{BD2}, r_{BD}: Geometry of the beamdump
Z_p: Atomic number of simulated ion in the loop
A: Mass number of simulated ion in the loop
θ: Angle of emission
KE: Kinetic energy
σ: Cross-section
Z_{max}: Highest atomic number in the imported data
A_{max}: Highest mass number in the imported data
X, X': Arrays for active and terminated trajectories
w_n, σ_n: Weight factor

Fig. 3. Flow chart of the ion-optical simulation code.

2.1. Magnetic field definition of superconducting solenoid magnet

The magnet used in the NEXT setup is from an old MRI scanner. It has a length of 157 cm, an inner diameter of 89 cm, and a magnetic field strength of 3 T at its center. The simulations require a realistic description of the magnetic field throughout the magnet including the fringe fields outside the magnet bore. Due to the symmetry of the

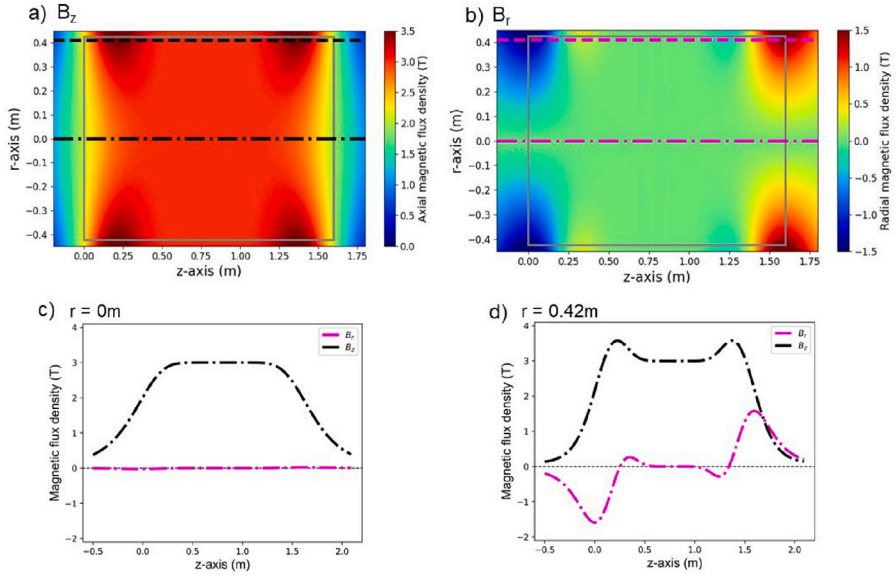

Fig. 4. Magnetic field of the solenoid modeled by the multipole expansion. (a) Map of the axial magnetic field, B_z, (b) Map of the radial magnetic field B_r. Magnetic flux density in axial and radial direction along (c) the central axis of the magnet and (d) near the magnet wall.

magnetic field, we can simply describe the fields as a function of the axial coordinate z and the radial coordinate r. A magnetic field map of this superconducting solenoid has been implemented in the simulation environment by using a multipole expansion [18] up to the 2nd order. This multipole expansion derived from the axial magnetic field component at the central axis allows a fast vectorized interpolations of the field at all positions.

In this method, a magnetic field that is symmetrical around the z-axis is defined by,

$$\mathbf{B} = B_r(r,z)\hat{\mathbf{r}} + B_z(r,z)\hat{\mathbf{z}} \tag{2}$$

in cylindrical coordinates (r, ϕ, z) [18]. The axial and radial components can be written as,

$$B_z(r,z) = \sum (-1)^n \frac{a_0^{(2n)}(z)}{(n!)^2}\left(\frac{r}{2}\right)^{2n}, \tag{3}$$

with

$$a_0(z) = B_z(0,z), \tag{4}$$

and

$$B_r(r,z) = \sum (-1)^{n+1} \frac{a_0^{(2n+1)}(z)}{(n+1)(n!)^2}\left(\frac{r}{2}\right)^{2n+1}, \tag{5}$$

where,

$$a_0^{(n)} = \frac{d^n a_0}{dz^n}. \tag{6}$$

The maps of the axial and the radial magnetic fields calculated with the expansion method are based on the provided axial magnetic field component at the central axis and are shown in Fig. 4 (a) and (b). Fig. 4 (c) and (d) show how the axial and radial fields evolve in z-direction along the central axis and at the edge of the bore of the magnet.

2.2. Distribution of atomic charge states

The trajectory of an ion recoiling out of the target through the solenoid magnet is determined by its initial inclination angle and magnetic rigidity. As mentioned in Section 1, the magnetic rigidity $B\rho$ of an ion depends on its velocity, its mass, and its atomic charge state. The masses and the velocities of the ions are provided by the theoretical prediction of the kinematics of the nuclear reaction. We implemented a calculation routine of the distribution of atomic charge states for all the ions (wanted and un-wanted transfer products as well as scattered beam and target material) in the code.

The atomic charge state of an ion depends on its atomic number (Z_p), its kinetic energy, and the atomic number of the target medium (Z_t) through which it passes. The ions of interest produced in ^{136}Xe+^{198}Pt have typically energies around 1.5 MeV/u to 3 MeV/u and have to pass through a ^{198}Pt target. The energy range of the transfermium isotopes produced in ^{48}Ca+^{251}Cf range from 0.1 MeV/u to 0.5 MeV/u and they pass through Cf-oxide layer of the target. To calculate the mean charge state, an empirical formula [19] has been implemented in the simulation code. This formula is based on several experimentally determined mean charge states, and is optimized for ions with proton numbers of $Z_p \geq 8$ and energies of $E < 6$ MeV/u within a precision of $\Delta\bar{q}/Z_p < 0.04$. Thus, it is suited for the energy regime of the ions of interest. The average charge state over the atomic number is defined as,

$$\bar{q}/Z_p = [1-e^{(-1.25Y+0.32Y^2-0.11Y^3)}][1-0.0019(Z_t-6)\sqrt{Y}+0.00001(Z_t-6)^2Y] \tag{7}$$

with

$$Y = \frac{v}{v' Z_p^{0.45}} \tag{8}$$

where v is the velocity of the ion, and $v' = 3.6 \cdot 10^8$ cm/s.

In order to calculate the width of the charge state distribution($d_{\bar{q}}$) within a precision of $\Delta d_{\bar{q}} < 20\%$, the following formula has been applied,

$$d_{\bar{q}} = d_0\sqrt{\bar{q}[1-(\bar{q}/Z_p)^{1/k}]} \tag{9}$$

where $k = 0.6$, $d_0 = 0.5$ as suggested in the Ref. [20].

The code samples the charge states from the normal distribution. Fig. 5 shows the calculated charge state distribution for ions of interest at various kinetic energies. The neutron-rich transfermium isotopes produced with actinide targets feature typically charges states ranging from +10 to +40. The atomic charge states of isotopes along $N = 126$ produced in ^{136}Xe-induced reactions range from +25 to +50. As the NEXT solenoid separator will be operated under vacuum at pressure of 10^{-5} mbar and lower, charge exchange reaction with residual gas can be neglected in the simulations.

Fig. 6 shows the impact of the charge state on the trajectories of the ion through the magnet. In general, higher charge states lead to a stronger bending of the ion trajectories within the magnetic field.

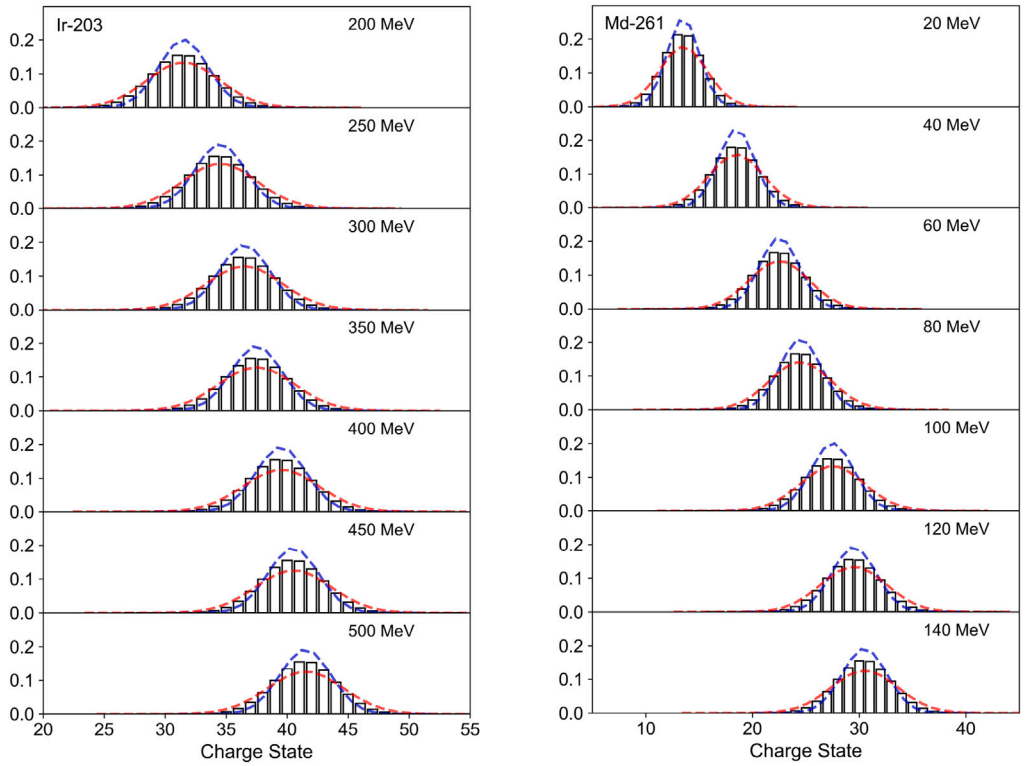

Fig. 5. Charge state distributions of ions of interest for various kinetic energies. The blue and red dashed lines illustrate a 20% error margin in the calculation of the charge state distribution width(Δd_q).

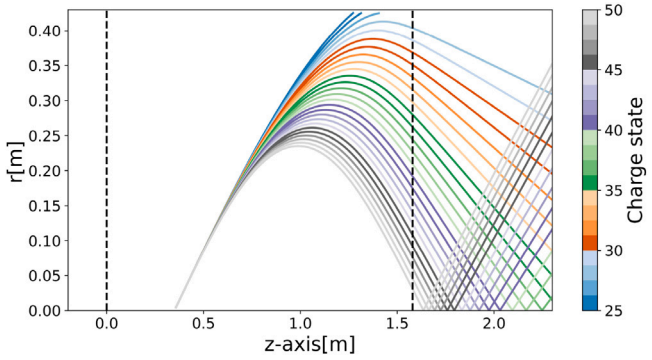

Fig. 6. Ion traces through the solenoid magnet. Dashed black lines indicate the dimensions of the magnet. The traces of ions with a charge state between 25 and 50 and a mass of 203 u are indicated. All ions have kinetic energies of 300 MeV and are emitted in angle of 30°.

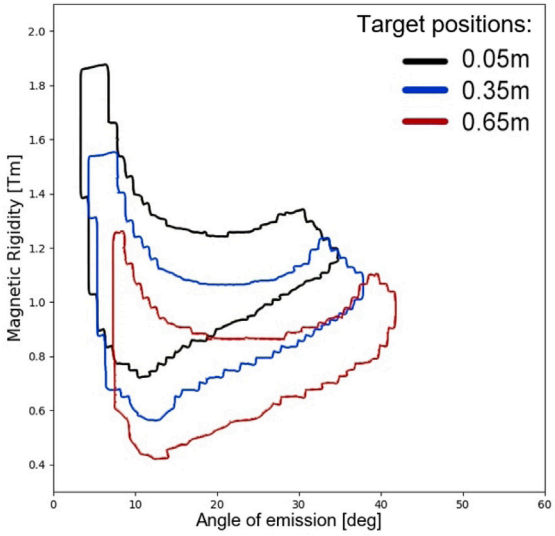

Fig. 7. Acceptance region for various positions of the target from where the ions are released. The position of the Faraday cup is 1.15 m and the position of the gas-catcher is 2.35 m. The magnetic field corresponds to the field map shown in Fig. 4.

3. Results of the simulation

The simulation code has been applied for a design study of the NEXT solenoid separator. For the design study we assumed just thin targets in which the energy loss and scattering is minor. The following obstacles have been implemented in the simulation: a target, a cylindrical Faraday cup of 38.5 cm length and 6.2 cm radius, and an aperture of the gas-catcher of 15 cm radius. The acceptance region of the solenoid separator was modified by adjusting the positions of these three components. The magnetic field was kept fixed at 3 T, the corresponding field map is shown in Fig. 4. At lower magnetic field strength the transmission efficiency was insufficient. The trajectories of the ions emitted from a point-like source (reaction target foil) at the central axis depend on only two variables: the angle and the magnetic rigidity. Thus, it is possible to calculate a 2D acceptance region for each layout of the system. Ions with an angle of emission and magnetic rigidity that are within the acceptance region, are transmitted from the target to the gas-catcher. Ions outside the acceptance region are suppressed. Fig. 7 shows the acceptance regions of the magnet for various positions of the target wheel. In the first step of the optimization of the setup, various combinations of the positions of the gas-catcher and of the target wheel were investigated for both reactions. In the second step these positions were fixed and the effect of the positioning of the Faraday cup was

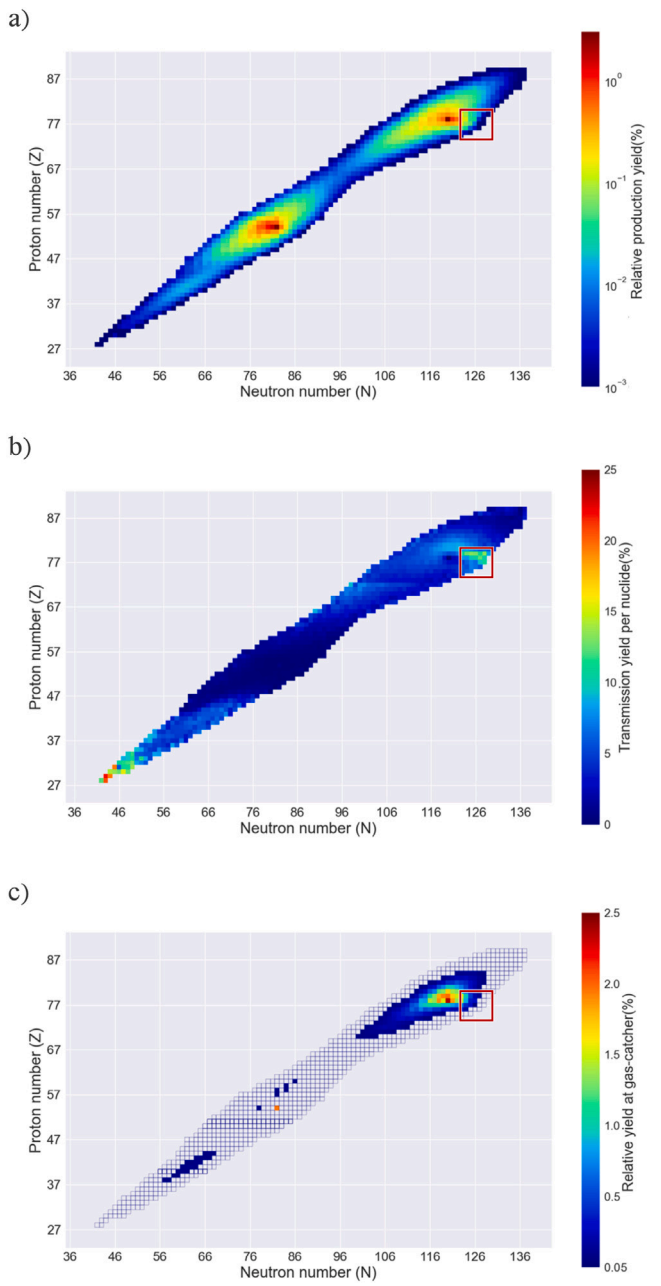

Fig. 8. (a) Relative production yield of the nuclides produced in the reaction ^{136}Xe+^{198}Pt normalized on the overall amount of scattered and produced nuclei. The region of interest around $N = 126$ is highlighted. (b) Transmission yield of each single nuclide through the solenoid separator from the target placed at 70 cm inside the magnet to the gas-catcher which is located 72 cm away from the magnet. Nuclei scattered with small inclination angle are stopped by the Faraday cup located 15 cm behind the target. (c) Relative yield of nuclides at the gas-catcher normalized on the total number of ions reaching the gas-catcher. Values below 0.05 are represented by the empty boxes.

investigated. In the following, we present the results of our studies of the two selected reactions.

3.1. ^{136}Xe+^{198}Pt

Fig. 8(a) shows the production yields of all the nuclides produced in ^{136}Xe+^{198}Pt. The region around $N = 126$ is highlighted. We selected ^{203}Ir, produced in the chosen reaction, for the optimization of the NEXT solenoid acceptance. Fig. 9 shows the distribution of the magnetic

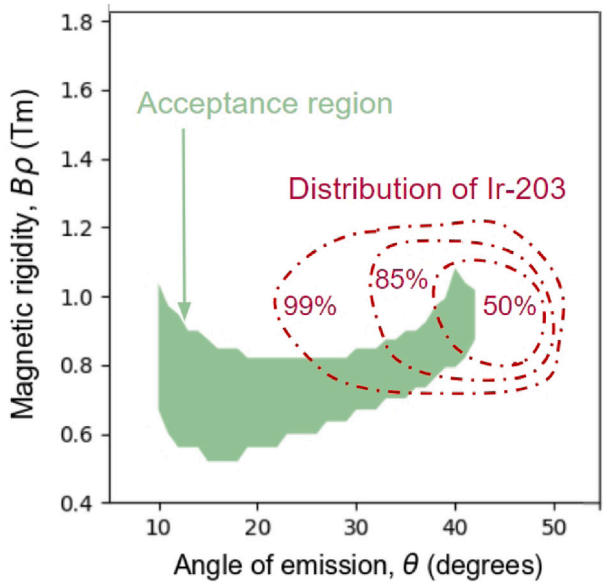

Fig. 9. Acceptance plot of the solenoid separator for ^{203}Ir. The green area indicates the acceptance region of the solenoid separator. Ions that are released from the target with the corresponding magnetic rigidity and angle of emission will reach the entrance window of the gas-catcher. The dashed, red lines indicate the distribution of the produced ions of ^{203}Ir.

rigidity and the angle of emission of the ions of ^{203}Ir as well as the acceptance region of the solenoid if the target is placed at 70 cm inside the solenoid magnet, the Faraday cup is 15 cm behind the target and the gas-catcher is located at a distance of 72 cm downstream from the magnet. These settings were found to be optimum and a transmission yield of around 7% of ^{203}Ir is achieved. This means that 7% of ^{203}Ir that is produced according to the theoretical prediction [13] will reach the gas-catcher. Assuming a target thickness of 1 mg/cm^2, the energy loss of the Xe-beam within the target will be around 0.2 MeV/u, which will push the emitting angle and velocity of ^{203}Ir-ion to slightly lower angles and lower velocity resulting in an increasing overlap with the acceptance region. Generally, the transmission efficiencies of isotopes around the $N = 126$ neutron-shell closure region range from 5% and 20%. A large fraction of the un-wanted by-products is sufficiently suppressed. Fig. 8(b) shows the transmission yields of each nuclide produced by the selected reaction. Assuming a beam current of 10^{11} ^{136}Xe ions per second and a target thickness of 1 mg/cm^2 ^{198}Pt, will result in a rate of around 81 kHz of ions including scattered beam and target material reaching the gas-catcher which is an acceptable rate for such a device (see e.g. [21]). Fig. 8 (c) shows the expected nuclide distribution at the gas-catcher. The ratio between nuclei around $N = 126$ (isotopes of platinum, iridium, osmium, and rhenium with $N = 124$ to $N = 128$, highlighted by the red box in Fig. 8 (c) to unwanted by products is around 1:22.

3.2. ^{48}Ca+^{251}Cf reaction

Fig. 10 (a) shows the production yield of the heavy transfer products of the reaction ^{48}Ca+^{251}Cf [14]. Only data for the heavy target-like transfer products were available for the simulations. Based on the reaction kinematics, it is expected that the major fraction of the projectile-like fragment will hit the wall of the magnet and not reaching the gas-catcher due to their magnetic rigidity and large angle of emission. The scattered primary beam and light fragments lie outside the acceptance regions shown in Fig. 11. The largest contribution to the background is predicted to come from scattered target material (Fig. 10 (a)). For the optimization, we selected the isotope ^{261}Md as the ion

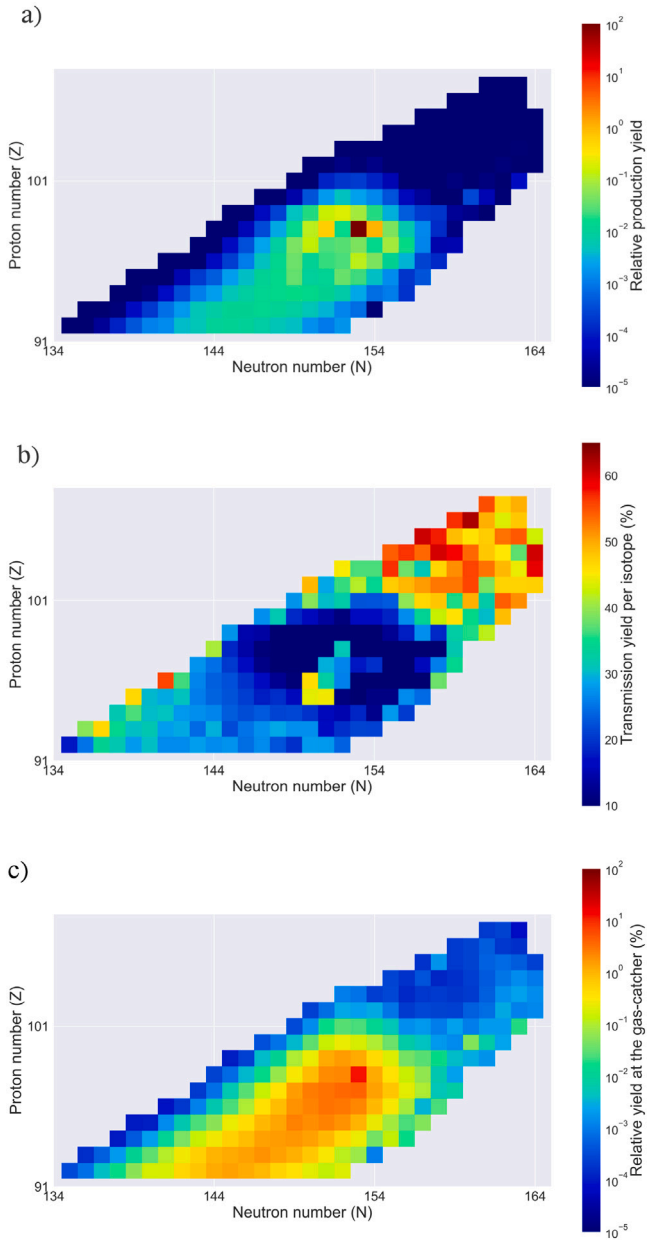

Fig. 10. (a) Relative yield of the heavy nuclides produced in the reaction ^{48}Ca+^{251}Cf normalized on the overall amount of scattered target material and produced nuclei above $Z > 90$. (b) Transmission yield of each single nuclide through the solenoid separator from the target placed 55 cm inside the magnet to the gas-catcher placed at 72 cm behind the magnet. Nuclei scattered in a small angle are stopped by the Faraday cup located 15 cm behind the target (c) Relative yield of the heavy nuclides normalized on the total amount of $Z > 90$ nuclei reaching at the gas-catcher.

of interest. Fig. 11 shows the angular distribution and the distribution of the magnetic rigidity of the ^{261}Md which are overlapping with the acceptance region of the solenoid separator placing the target 55 cm inside the magnet and the gas catcher 72 cm behind the magnet. Thus, high transmission efficiencies of around 50% and higher are reached for heavy transfer products (see Fig. 10 (b)). Scattered target material and transfer products with similar masses as the target nucleus are successfully suppressed as indicated by the blue colors in Fig. 10 (b). Assuming a beam current of 10^{11} ^{48}Ca ions per second and a target thickness of 0.5 mg/cm^2 ^{251}Cf, around 500 ions per second of scattered target material will reach the entrance window of the gas-catcher. The ratio of neutron-rich ions of interest around $Z = 101$ and $N = 162$

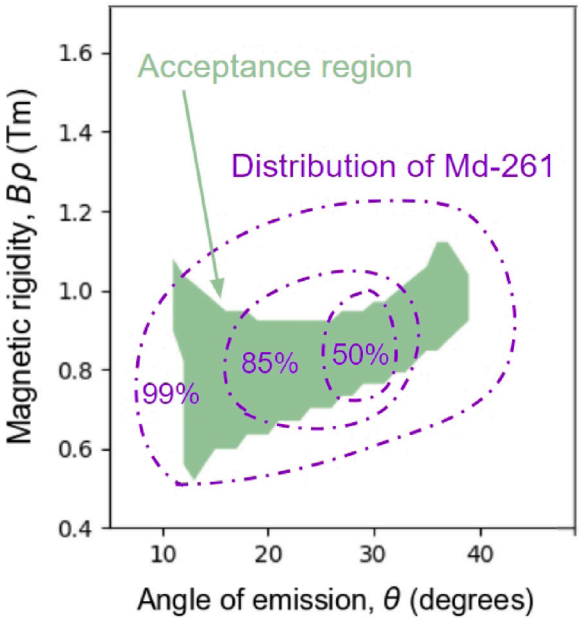

Fig. 11. Acceptance plot of the solenoid separator for ^{261}Md. The green area indicates the acceptance region of the solenoid separator. Ions that are released from the target with the corresponding magnetic rigidity and angle of emission will reach the entrance window of the gas-catcher. The dashed lines show the distribution of the produced ions of ^{261}Md.

to the remaining heavy products (unwanted-proton-rich and close to target nuclei) improves by a factor of 200 comparing Fig. 10 (a) and (c).

4. Conclusion

A Python code has been developed to simulate the ion traces through a solenoid magnetic field. The code allows to determine the acceptance region of any solenoid separator and is thus a crucial tool for planning of experiments using various target and beam combinations. With the code the optimal positions of the components of any solenoid separators can be calculated based on the acceptance region of such a device. The simulation code is capable to read in input files containing differential cross sections, kinetic energies, and angle of emission of ions and to calculate automatically their charge states.

We used the code for initial design studies of the NEXT solenoid separator. In order to optimize the longitudinal position of the components of the separator, we selected two MNT reactions ^{136}Xe+^{198}Pt at 6 MeV/u to produce nuclei around $N = 126$ shell closure and ^{48}Ca+^{251}Cf to investigate neutron-rich transfermium nuclei. Based on our simulations, we determined a fixed position of the gas-catcher around 70 cm to 80 cm downstream from the magnet that is suited for both reactions. We found the distance of 15 cm between the target and the Faraday cup as a good balance to suppress background and still achieve sufficient transmission yields of the isotopes of our interest. Within the NEXT, the position of the target wheel is adjustable inside the magnet in order to shape the acceptance region. Based on our simulation, transmission yields of around 5% to 20% for nuclei around $N = 126$ in the reaction ^{136}Xe+^{198}Pt are realistic. For heavy neutron-rich transfermium isotopes produced in ^{48}Ca+^{251}Cf, transmission yields above 50% are achievable.

CRediT authorship contribution statement

A. Soylu: Writing – original draft, Visualization, Validation, Software, Investigation. **X. Chen:** Writing – review & editing, Validation. **J.**

Even: Writing – review & editing, Supervision, Project administration, Methodology, Investigation, Funding acquisition, Conceptualization. **A. Karpov:** Validation, Data curation. **V. Saiko:** Data curation. **J. Sarén:** Writing – review & editing, Software, Methodology, Formal analysis, Data curation. **J. Uusitalo:** Writing – review & editing, Methodology.

Declaration of competing interest

The authors declare the following financial interests/personal relationships which may be considered as potential competing interests: Julia Even reports financial support was provided by European Research Council. Arif Soylu reports financial support was provided by European Research Council. Xiangcheng Chen reports financial support was provided by European Research Council. If there are other authors, they declare that they have no known competing financial interests or personal relationships that could have appeared to influence the work reported in this paper.

Data availability

Data will be made available on request.

Acknowledgments

We gratefully acknowledge funding from the European Research Council (ERC) under the European Union's Horizon 2020 research and innovation programme (ERC-2018-STG, Grant agreement ID: 803740).

References

[1] W.D. Loveland, The synthesis of new neutron-rich heavy nuclei, Front. Phys. 7 (2019) 23.
[2] L. Corradi, et al., Multinucleon transfer reactions studied with the heavy-ion magnetic spectrometer PRISMA, Eur. Phys. J. A 25 (1) (2005) 427–428.
[3] C. Golabek, et al., Investigation of deep inelastic reactions in ^{238}U+ ^{238}U at Coulomb barrier energies, Eur. Phys. J. A 43 (3) (2010) 251–259.
[4] Y.X. Watanabe, et al., Study of collisions of ^{136}Xe+ ^{198}Pt for the KEK isotope separator, Nucl. Instrum. Methods Phys. Res. B 317 (2013) 752–755.
[5] G. Savard, M. Brodeur, J. Clark, R. Knaack, A. Valverde, The N = 126 factory: A new facility to produce very heavy neutron-rich isotopes, Nucl. Instrum. Methods Phys. Res. B 463 (2020) 258–261.
[6] T. Dickel, et al., Multi-nucleon transfer reactions at ion catcher facilities - a new way to produce and study heavy neutron-rich nuclei, J. Phys. Conf. Ser. 1668 (1) (2020) 012012.
[7] M. Götz, et al., Radiochemical study of the kinematics of multi-nucleon transfer reactions in ^{48}Ca+ ^{248}Cm collisions 10% above the Coulomb barrier, Nucl. Phys. A 961 (2017) 1–21.
[8] A. Mollaebrahimi, et al., A setup to develop novel chemical isobaric separation (CISE), Nucl. Instrum. Methods Phys. Res. B 463 (2020) 508–511.
[9] X. Chen, et al., Stacked-ring ion guide for cooling and bunching rare isotopes, Int. J. Mass Spectrometr. 477 (2022) 116856.
[10] R. Wolf, et al., ISOLTRAP's multi-reflection time-of-flight mass separator/spectrometer, Int. J. Mass Spectrometr. 349 (2013) 123–133.
[11] M. Schlaich, et al., A multi-reflection time-of-flight mass spectrometer for the offline ion source of the PUMA experiment, Int. J. Mass Spectrometr. 495 (October 2023) (2024) 117166.
[12] G. Van Rossum, F.L. Drake, Python 3 Reference Manual, CreateSpace, Scotts Valley, CA, 2009.
[13] A. Karpov, V. Saiko, Production of neutron-rich nuclides in the vicinity of N = 126 shell closure in multinucleon transfer reactions, EPJ Web Conf. 163 (2017) 00027.
[14] A. Karpov, V. Saiko, Synthesis of transuranium nuclei in multinucleon transfer reactions at near-barrier energies, Phys. Particles Nuclei Lett. 16 (6) (2019) 667–670.
[15] J.F. Ziegler, M.D. Ziegler, J.P. Biersack, SRIM - The stopping and range of ions in matter (2010), Nuclear Instrum. Methods Phys. Res. Section B: Beam Interact. Mater. Atoms 268 (11–12) (2010) 1818–1823.
[16] K.E. Atkinson, An introduction to numerical analysis, John Wiley & Sons, 2008, p. 418 433.
[17] C.H. Harris, et al., Array programming with NumPy, Nature 585 (7825) (2020) 357–362.
[18] K.T. McDonald, Expansion of an axially symmetric, static magnetic field in terms of its axial field, 2024, available at http://kirkmcd.princeton.edu/examples/axial.pdf. (Accesed on 10 January 2024).
[19] K. Shima, T. Ishihara, T. Mikumo, Empirical formula for the average equilibrium charge-state of heavy ions behind various foils, Nucl. Instrum. Methods Phys. Res. 200 (2) (1982) 605–608.
[20] V. Nikolaev, I. Dmitriev, On the equilibrium charge distribution in heavy element ion beams, Phys. Lett. A 28 (4) (1968) 277–278.
[21] J. Neumayr, et al., The ion-catcher device for SHIPTRAP, Nucl. Instrum. Methods Phys. Res. B 244 (2) (2006) 489–500.